JOURNAL OF PROPULSION AND POWER
Vol. 17, No. 3, May–June 2001

On the Breakup of Viscous Liquid Sheets by Dual-Mode Linear Analysis

Sushanta K. Mitra,* Xianguo Li,† and Metin Renksizbulut†
University of Waterloo, Waterloo, Ontario, N2L 3G1, Canada

The breakup of plane viscous liquid sheets moving in a gas stream has been studied. A dual-mode linear stability analysis has been carried out under the combined influence of sinuous and varicose modes of disturbances at the two liquid–gas interfaces. The effect of various parameters, such as the Reynolds number, Weber number, density ratio, velocity ratio, and the phase angle between the two modes, on the breakup characteristics of the liquid sheets has been investigated. At wavelengths corresponding to the dominant wavelengths for either the sinuous or the varicose mode, the breakup of the liquid sheet occurs at full-wavelength intervals, but the breakup point shifts between the half- and the full-wavelength when the respective dominant wavelengths corresponding to the sinuous and the varicose modes are applied simultaneously. The breakup time decreases as the proportion of the varicose mode is increased in the initial disturbance imposed on the liquid sheets. The breakup length (or time) decreases with an increase in the Reynolds number, Weber number, density ratio, and velocity ratio. The sheet profiles change for different values of Weber number, density ratio, velocity ratio, and the phase angle between the two modes. Comparison with experimental results shows that the present analysis is able to match the interface profile close to the nozzle exit, but not further downstream where nonlinear effects are predominant.

Nomenclature

a	=	half-sheet thickness
k	=	wave number
k_s	=	wave number for sinuous mode
k_v	=	wave number for varicose mode
L_b	=	sheet breakup length
p	=	dimensionless pressure
Re	=	Reynolds number
t	=	time
U	=	velocity ratio (U_g/U_ℓ)
We	=	Weber number
x	=	spatial coordinate along x direction
y	=	spatial coordinate along y direction
ϵ_1	=	weighting factor for sinuous mode
ϵ_2	=	weighting factor for varicose mode
η	=	interface deformation
η_0	=	initial disturbance amplitude
θ	=	phase angle
ρ	=	density ratio (ρ_g/ρ_ℓ)
σ	=	surface tension
ψ	=	stream function
ω	=	complex eigenfrequency

Subscripts

g	=	gas phase
j	=	interface location (1, upper; 2, lower)
ℓ	=	liquid phase

Introduction

IN many liquid atomization processes liquid is continuously ejected from a nozzle in the form of a thin sheet. Unstable surface waves develop and grow along the interface, which eventually leads to the breakup of the sheet into a multitude of droplets of different sizes and velocities. Sprays are used extensively in various industrial applications ranging from spray cooling, drying, coating, agriculture, chemical processes to power generation and propulsion systems. Clearly, a sound knowledge of the sheet disintegration process is essential for the design and operation of practical spray systems. For gas-turbine applications, where mostly air-assist and air-blast atomizations are employed, the liquid to be atomized is typically in the form of a thin annular sheet. A number of previous studies[1,2] indicate that the curvature effect might be negligible, and hence a plane liquid sheet model can be adopted in the study of the atomization process.[3] Therefore, the present work focuses on the breakup of plane liquid sheets in a surrounding gas stream.

Previous stability analyses of inviscid liquid sheets[4,5] indicate that two independent modes of unstable waves exist at the liquid–gas interface: an antisymmetric wave or the so-called sinuous mode and a symmetric wave or varicose mode. The temporal instability analysis of a viscous liquid sheet[6] shows that liquid viscosity introduces an additional temporal mode, named therein as viscosity-enhanced instability, which destabilizes a range of wave numbers. However, at high Weber numbers of practical importance liquid viscosity tends to reduce the disturbance growth rate. The absolute and spatial instability have also been investigated.[7–9] The absolute instability for a plane liquid sheet only occurs at Weber numbers less than about one, a situation unlikely to occur under practical conditions in atomization, although it is relevant to other applications such as coating. It is also known that the spatial and the temporal instabilities are related to each other by Gaster's relation[10] for liquid sheets with large Weber numbers[8]; although in general Gaster's relation is only valid near the neutrally stable cutoff wave numbers.[10] A summary of the linear stability analysis for the liquid sheets[11] shows that the sinuous mode is more unstable, and it tends to grow faster under practical conditions of large Weber numbers. Hence the stability characteristics of the sinuous mode (i.e., a single-mode) has often been used to predict the breakup characteristics of liquid sheets and the sizes of the subsequently formed droplets.

However, such a linear stability analysis of plane liquid sheets subject only to the sinuous mode of disturbance fails to produce the breakup of liquid sheets because the two liquid-gas interfaces remain at a constant distance apart during the growth of the unstable sinuous waves. As a remedy, nonlinear stability analysis[12–14] has been conducted to obtain the breakup of plane liquid sheets. A perturbation scheme[14] was used with the sinuous mode as the initial condition of disturbance. The sheet breakup is primarily caused by the presence of the varicose mode appearing in the second-order

Received 26 January 2000; revision received 2 June 2000; accepted for publication 17 August 2000.

*Graduate Student, Department of Mechanical Engineering.
†Professor, Department of Mechanical Engineering.

solution (the harmonic), and hence the breakup of the liquid sheet occurs at about half-wavelength interval. The growth of the fundamental sinuous mode results in the large amplitude deformation of the liquid-sheet, whereas the harmonic varicose mode brings the two interfaces close together causing the liquid sheet to breakup. Therefore, even though the harmonic varicose mode has much smaller growth rate (the second-order effect) than the fundamental sinuous mode (the first-order effect), it is the cause of the sheet disintegration. This brings out the necessity of investigating the case of fundamental varicose mode as the initial condition because its first-order effects can dominate the breakup process. As a result, a nonlinear stability analysis has been carried out with the varicose mode as the initial disturbance.[15] It is found that when a varicose disturbance is initially applied the liquid sheet breaks up at full-wavelength interval in contrast to half-wavelength interval for an initial sinuous disturbance, and under certain conditions of practical importance the breakup process is dictated by the fundamental varicose mode rather than its sinuous counterpart. Hence, the fundamental varicose mode cannot be discarded for the study of liquid-sheet breakup process.

In reality, both the fundamental sinuous and varicose modes are unstable, and they grow simultaneously. Thus the present work studies the breakup process of plane liquid sheets by applying both the sinuous and the varicose modes of disturbance on the two liquid–gas interfaces as the initial condition. As a first step, the breakup process is investigated by means of linear stability analysis, and the details are discussed next. An application of the linear theory to predict the sheet breakup is instructive only because the breakup phenomena are inherently nonlinear.

Analysis

Figure 1 shows a schematic diagram of a two-dimensional viscous liquid sheet of uniform thickness $2a$ moving with a uniform velocity U_ℓ into a surrounding inviscid and incompressible gaseous medium, which itself is moving with a uniform velocity of U_g. The density of the gas and the liquid phases are ρ_g and ρ_ℓ and the viscosity of the liquid is μ_ℓ. Gas viscosity in general reduces the disturbance growth rate, but does not alter the characteristics of the disturbances.[9]

On the liquid–gas interfaces disturbances are present in the form of sinuous and varicose waves with a phase angle θ between them. To simplify the presentation, physical parameters are nondimensionalized using the half-sheet thickness a, the convection time a/U_ℓ, and the liquid density ρ_ℓ. Therefore, the initial condition for the surface deformation $\eta_j(x, t)$ can be written as

$$\eta_j(x, 0) = \eta_0[\epsilon_1 \cos(kx) + (-1)^{j+1}\epsilon_2 \cos(kx + \theta)] \qquad (1)$$

where $j = 1, 2$ refers to the upper and lower interface, respectively; ϵ_1 and ϵ_2 are the weighting factors denoting a pure sinuous wave for $\epsilon_1 = 1$ and $\epsilon_2 = 0$, and a pure varicose wave for $\epsilon_1 = 0$ and $\epsilon_2 = 1$; k is the wave number related to the wavelength λ by $k = 2\pi/\lambda$; and η_0 is the initial amplitude of interfacial disturbance. A stream-function formulation is adopted for the entire flowfield so that the dimensionless stream functions ψ and the surface deformation $\eta_j(x, t)$ must

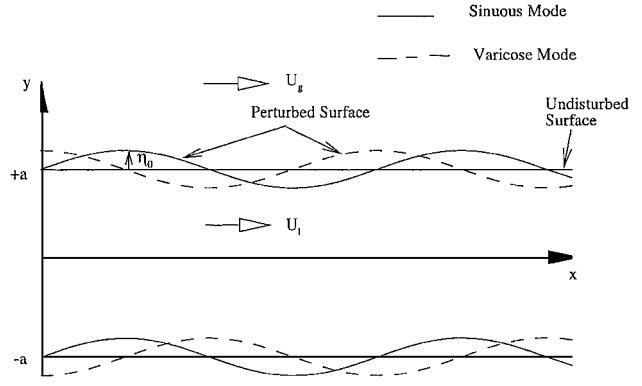

Fig. 1 Schematic of a plane liquid sheet subjected to a combination of sinuous and varicose disturbances.

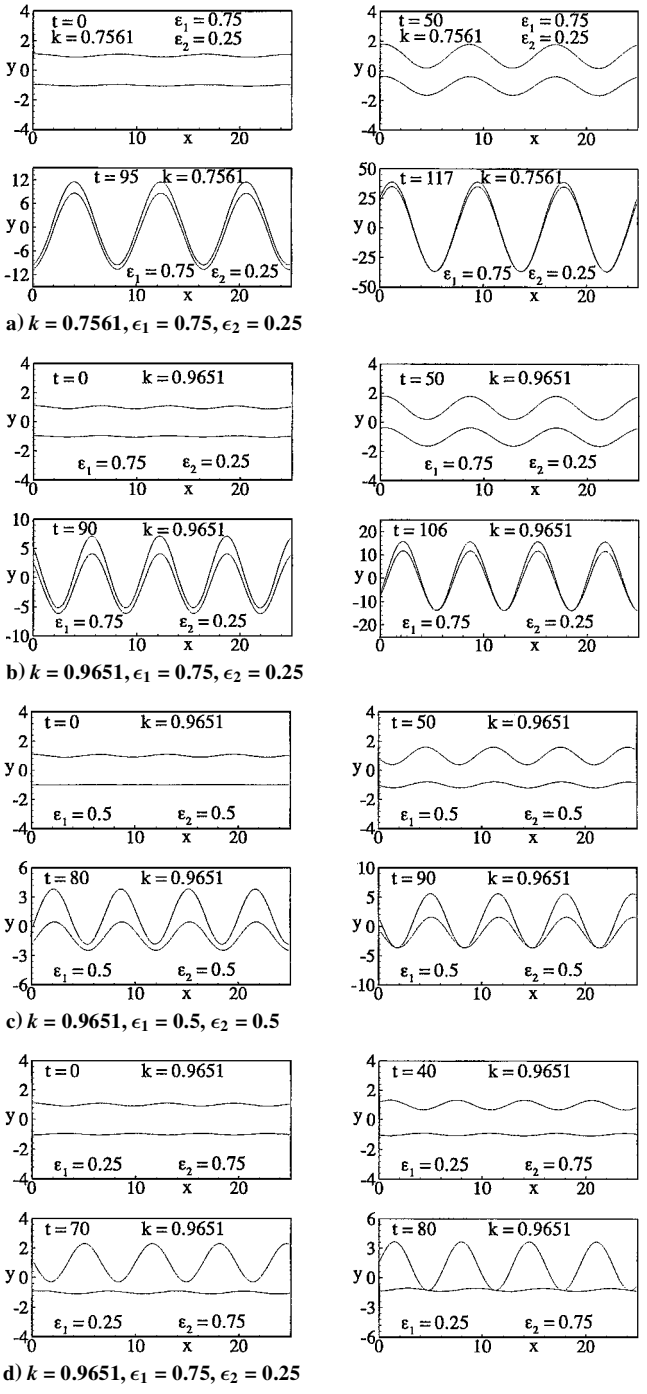

Fig. 2 Evolution of surface deformation at the dominant wave number for $We = 150$, $Re = 2 \times 10^3$, $\rho = 0.001$, $U = 4$, $\theta = 0$, $\eta_0 = 0.1$.

satisfy the following linearized Navier–Stokes equation for the gas and the liquid phases:

$$\nabla^2\left(\frac{\partial}{\partial t} + U\frac{\partial}{\partial x}\right)\psi_g = 0 \qquad \text{for} \qquad \begin{cases} 1 + \eta_1 \le y < +\infty \\ -\infty < y \le -1 + \eta_2 \end{cases} \qquad (2)$$

$$\nabla^2\left[\left(\frac{\partial}{\partial t} + U\frac{\partial}{\partial x}\right) - \frac{1}{Re}\nabla^2\right]\psi = 0$$

$$\text{for} \qquad -1 + \eta_2 \le y \le 1 + \eta_1 \qquad (3)$$

and the boundary conditions applied at $y = (-1)^{j+1} + \eta_j$ are

$$\psi_x + \eta_{j,t} + \psi_y \eta_{j,x} = 0 \qquad (4)$$

$$\psi_{g,x} + \eta_{j,t} + \psi_{g,y}\eta_{j,x} = 0 \qquad (5)$$

$$\frac{1}{Re}(\psi_{yy} - \psi_{xx}) = 0 \tag{6}$$

$$p - p_g + \frac{2}{Re}\psi_{x,y} = \frac{(-1)^j \eta_{j,xx}}{We\left(1 + \eta_{j,x}^2\right)^{3/2}} \tag{7}$$

Further in the ambient gas and far away from the liquid sheet, the effects of disturbances should remain bounded, that is,

$$\psi_g \quad \text{and} \quad p_g \quad \text{bounded as} \quad y \to \pm\infty \tag{8}$$

In the preceding equations the Reynolds and Weber numbers and the dimensionless velocity and density ratios are defined as

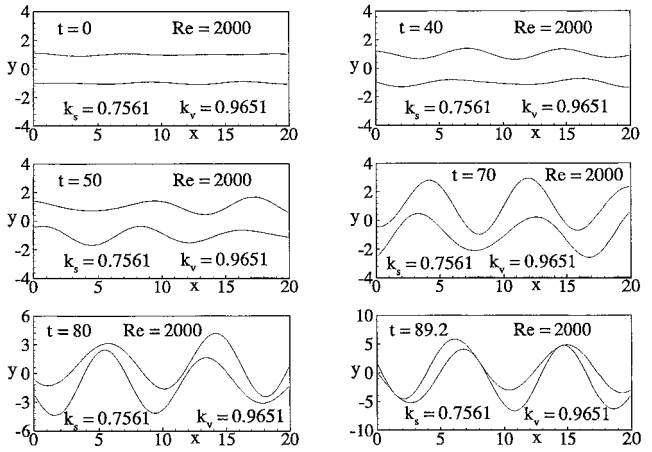

Fig. 3 Evolution of surface deformation for $We = 150$, $Re = 2 \times 10^3$, $\rho = 0.001$, $U = 4$, $\theta = 0$, $\eta_0 = 0.1$, $\epsilon_1 = 0.5$, $\epsilon_2 = 0.5$, $k_s = 0.7561$, and $k_v = 0.9651$.

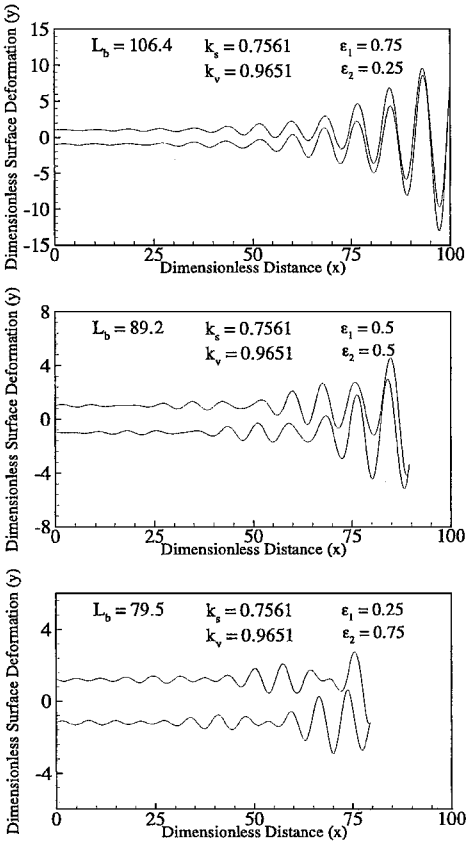

Fig. 4 Spatial surface deformation for $We = 150$, $Re = 2 \times 10^3$, $\rho = 0.001$, $U = 4$, $\theta = 0$, $\eta_0 = 0.1$, $k_s = 0.7561$, $k_v = 0.9651$, and different values of ϵ_1 and ϵ_2.

$$Re = \rho_\ell U_\ell a/\mu_\ell; \qquad We = \rho_\ell U_\ell^2 a \Big/ \sigma$$
$$U = U_g/U_\ell; \qquad \rho = \rho_g/\rho_\ell \tag{9}$$

and p and p_g are the dimensionless pressure in the liquid and gas phase, respectively; and to be determined from the momentum equations, thus involving the density ratio ρ in the gas-phase pressure p_g. The subscripts t, x, y represent the partial derivatives with respect to time and the spatial coordinates x and y, respectively. Equations (4) and (5) are the kinematic boundary conditions stating that the fluid particles initially on the interfaces will remain there subsequently. Equations (6) and (7) are the dynamic boundary conditions stating that the shear stress at the interfaces vanishes and the difference in the normal stress across the free surface is caused by the surface tension effect.

Because the boundary conditions are applied at $y = (-1)^{j+1} + \eta_j(x, t)$ where $\eta_j(x, t)$ is not known a priori, the stream functions ψ and ψ_g at $y = (-1)^{j+1} + \eta_j$ are expanded into a Taylor series at $y = (-1)^{j+1}$ and the linearized boundary conditions become

$$\psi_x + \eta_{j,t} + \eta_{j,x} = 0 \tag{10}$$

$$\psi_{g,x} + \eta_{j,t} + U\eta_{j,x} = 0 \tag{11}$$

$$(1/Re)(\psi_{yy} - \psi_{xx}) = 0 \tag{12}$$

$$p - p_g + (2/Re)\psi_{x,y} - [(-1)^j/We]\eta_{j,xx} = 0 \tag{13}$$

A wave-form solution is sought for the stream functions from the governing Eqs. (2) and (3). With the known disturbance velocity field the disturbance pressures are obtained from the momentum equations for the gas and the liquid phases. Substitution of these

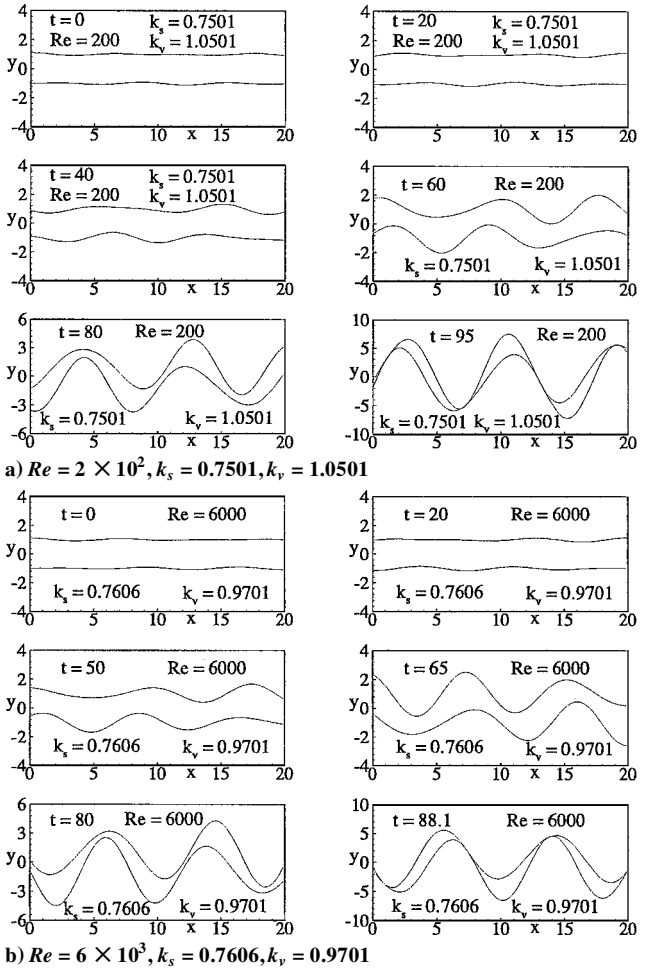

a) $Re = 2 \times 10^2$, $k_s = 0.7501$, $k_v = 1.0501$

b) $Re = 6 \times 10^3$, $k_s = 0.7606$, $k_v = 0.9701$

Fig. 5 Evolution of surface deformation for $We = 150$, $\rho = 0.001$, $U = 4$, $\theta = 0$, $\eta_0 = 0.1$, $\epsilon_1 = \epsilon_2 = 0.5$.

results into the boundary conditions Eqs. (10–13) and (8) leads to the following dispersion relations between the complex eigenfrequency ω and disturbance wave number k (Ref. 16):

Sinuous:

$$[(\omega+ik)+2k^2/Re]^2\tanh(k)-(4k^3/Re^2)S_a\tanh(S_a)$$
$$+\rho(\omega+ikU)^2+k^3/We=0 \tag{14}$$

Varicose:

$$[(\omega+ik)+2k^2/Re]^2\coth(k)-(4k^3/Re^2)S_a\coth(S_a)$$
$$+\rho(\omega+ikU)^2+k^3/We=0 \tag{15}$$

where $S_a=\sqrt{[k^2+Re(\omega+ik)]}$. From the dispersion relations complex solutions of ω are obtained for any given real wave number k along with the specified flow parameters. Because the dispersion relations cannot be solved analytically in closed form, a numerical procedure has been performed through Muller's method.[17] After solving the dispersion relations, along with the initial condition for the surface deformation stated in Eq. (1), the evolution of the surface deformation becomes

$$\eta_j(x,t)=\eta_0[\epsilon_1\cosh(\omega_1 t)\cos(\alpha_1 t+kx)$$
$$+(-1)^{j+1}\epsilon_2\cosh(\omega_2 t)\cos(\alpha_2 t+kx+\theta)] \tag{16}$$

Here, ω_1 and ω_2 are the real part of ω obtained by solving Eqs. (14) and (15), and they represent the growth rate for the sinuous and varicose modes, respectively; α_1 and α_2, the imaginary part of ω, are the corresponding angular frequency. Typical values of ω_1, ω_2, α_1, and α_2 for different flow conditions are given in Table 1. The wave number k appearing in two places in Eq. (16), one associated with the sinuous mode and the other with the varicose mode, and they are not necessarily the same. This will be discussed in details in the following section.

Results and Discussion

Figure 2 shows the surface deformation at different time instants according to Eq. (16) for the physical parameters of $We=150$, $Re=2000$, $\rho=0.001$, $U=4.0$, $\theta=0$, and $\eta_0=0.1$. The values of We, Re, ρ, and U chosen here correspond to water sheets in air typically encountered in laboratory experiments. Figure 2 is composed of four different cases, and each case is represented by four difference sequences in time t as the disturbance propagates. The wave number $k=0.7561$ in Fig. 2a is the dominant wave number for the sinuous mode, determined from Eq. (14). The dominant wave number corresponds to the mode of maximum instability (i.e., the maximum disturbance growth rate). The proportion of the sinuous and the varicose disturbances initially at the two liquid–gas

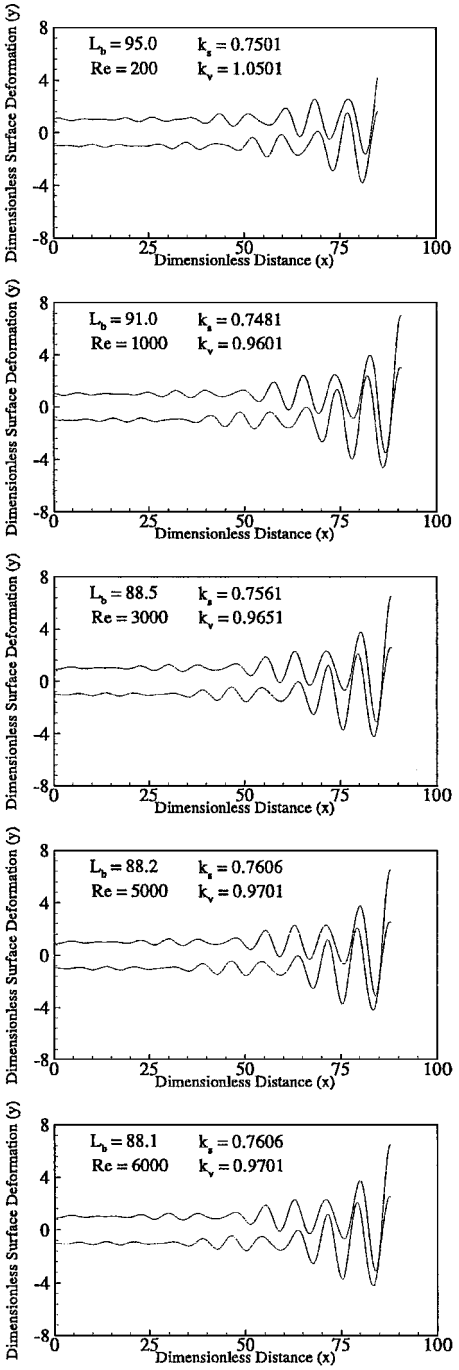

Fig. 6 Spatial surface deformation for $We=150$, $\rho=0.001$, $U=4$, $\theta=0$, $\eta_0=0.1$, $\epsilon_1=\epsilon_2=0.5$, and different values of Reynolds numbers.

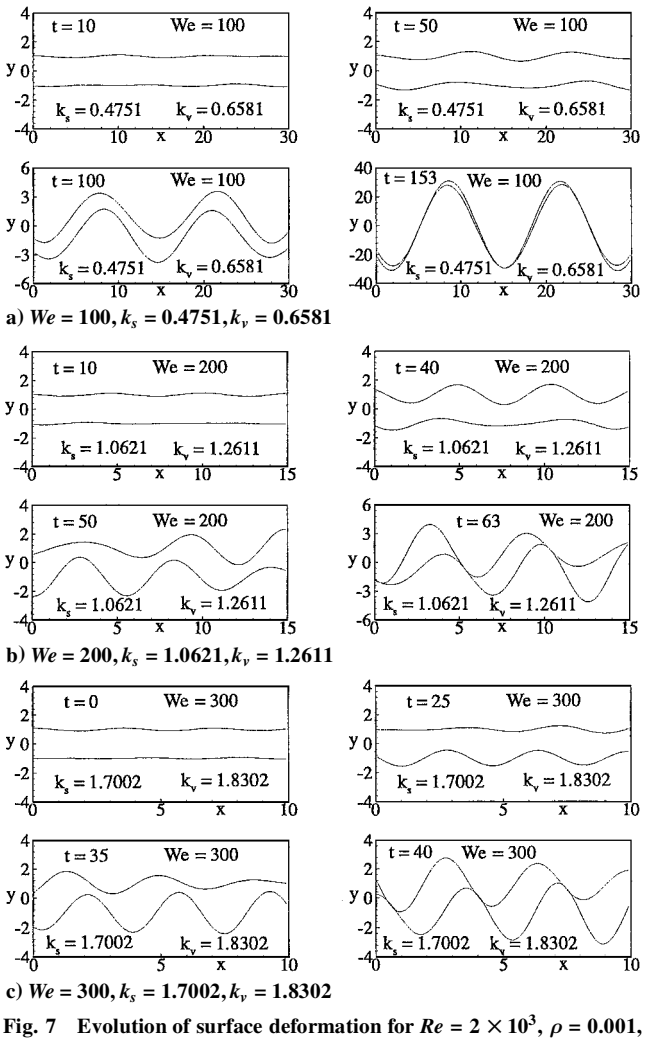

Fig. 7 Evolution of surface deformation for $Re=2\times10^3$, $\rho=0.001$, $U=4$, $\theta=0$, $\eta_0=0.1$, $\epsilon_1=\epsilon_2=0.5$.

Table 1 Values of $\omega_1, \omega_2, \alpha_1, \alpha_2, k_s$, and k_v for different flow conditions.

Re	*We*	ρ	*U*	k_s	k_v	ω_1	α_1	ω_2	α_2
200	150	0.001	4.0	0.7501	1.0501	5.7030*e*−2	−7.4631*e*−1	3.9126*e*−2	−1.0378
1000	150	0.001	4.0	0.7481	0.9601	5.8507*e*−2	−7.5089*e*−1	4.0756*e*−2	−9.6110*e*−1
2000	150	0.001	4.0	0.7561	0.9651	5.8899*e*−2	−7.5936*e*−1	4.1394*e*−2	−9.6683*e*−1
3000	150	0.001	4.0	0.7561	0.9651	5.9046*e*−2	−7.5948*e*−1	4.1633*e*−2	−9.6702*e*−1
6000	150	0.001	4.0	0.7606	0.9701	5.9204*e*−2	−7.6408*e*−1	4.1889*e*−2	−9.7219*e*−1
2000	100	0.001	4.0	0.4751	0.6581	4.6210*e*−2	−4.7816*e*−1	2.4176*e*−2	−6.5906*e*−1
2000	200	0.001	4.0	1.0621	1.2611	7.1669*e*−2	−1.0656	5.9016*e*−2	−1.2635
2000	300	0.001	4.0	1.7002	1.8302	9.9060*e*−2	−1.7039	9.3331*e*−2	−1.8332
2000	150	0.002	4.0	1.7012	1.8337	1.4052*e*−1	−1.7107	1.3252*e*−1	−1.8424
2000	150	0.005	4.0	4.3879	4.4105	5.2928*e*−1	−4.4434	5.2912*e*−1	−4.4660
2000	150	0.008	4.0	6.9847	6.9847	1.0560	−7.1214	1.0560	−7.1242
2000	150	0.002	3.0	0.3080	0.4433	2.4667*e*−2	−3.1003*e*−1	9.0661*e*−3	−4.4359*e*−1
2000	150	0.002	6.0	2.4378	2.4963	2.2432*e*−1	−2.4474	2.2102*e*−1	−2.5056
2000	150	0.002	8.0	4.8005	4.8005	6.0524*e*−1	−4.8236	6.0515*e*−1	−4.8235

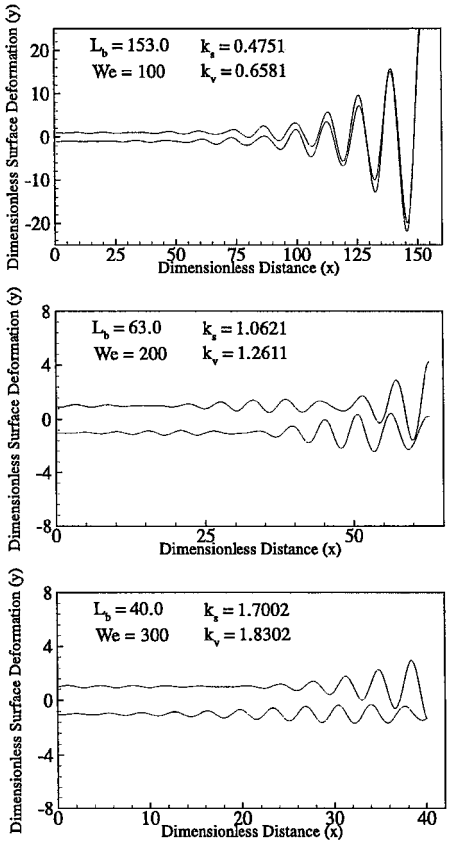

Fig. 8 Spatial surface deformation for $Re = 2 \times 10^3$, $\rho = 0.001$, $U = 4$, $\theta = 0$, $\eta_0 = 0.1$, $\epsilon_1 = \epsilon_2 = 0.5$, and different value of Weber numbers.

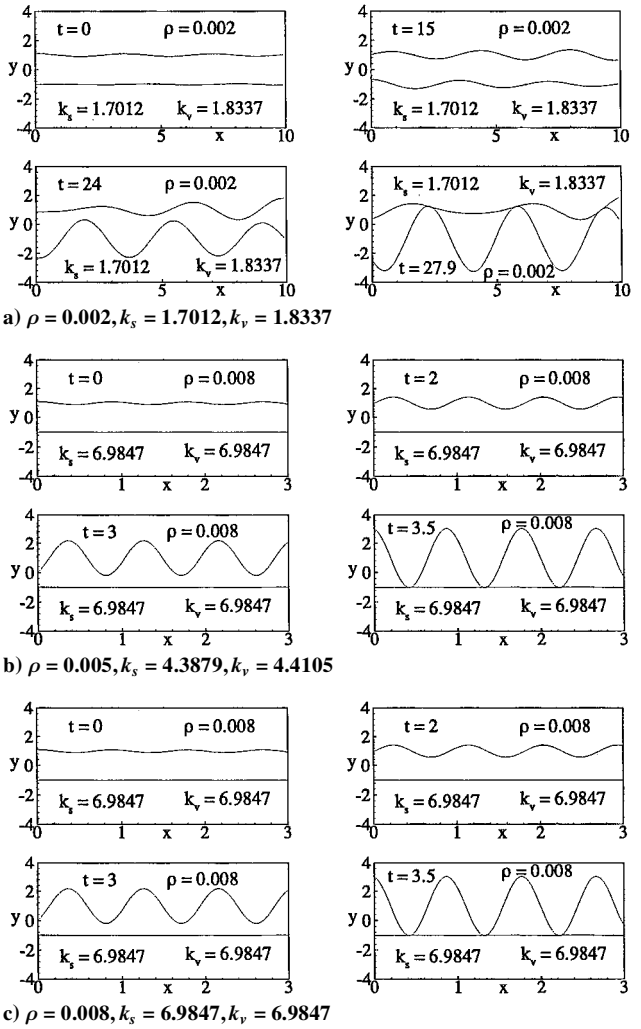

Fig. 9 Evolution of surface deformation for $We = 150$, $Re = 2 \times 10^3$, $U = 4$, $\theta = 0$, $\eta_0 = 0.1$, $\epsilon_1 = \epsilon_2 = 0.5$.

interfaces are $\epsilon_1 = 0.75$ and $\epsilon_2 = 0.25$, respectively. The two interfaces remain almost at a constant distance apart for the majority of time, with the sheet thinning starting at about $t = 95$ and the sheet breakup at $t = 117$. Clearly, the present linear stability analysis predicts the breakup of the liquid sheet. The breakup occurs at the full-wavelength interval, similar to the breakup process caused by the varicose mode alone.[15] Figure 2b shows the surface evolution for $k = 0.9651$, which corresponds to the dominant wave number for the varicose mode, determined from Eq. (15). The other physical parameters remain the same as in Fig. 2a. The breakup time and the wave amplitude at the breakup point are reduced compared to Fig. 2a. This shows that the varicose mode is causing the sheet to breakup early and also to reduce the wave growth. These are more evident in Fig. 2c, where the proportion of the varicose mode is increased to 50% compared to 25% in Fig. 2b, keeping all other parameters unchanged. Further reduction in breakup time is observed in Fig. 2d, where $\epsilon_1 = 0.25$ and $\epsilon_2 = 0.75$ and the wave amplitude at the breakup is also substantially reduced. However, because of the large proportion of varicose mode the upper interface tends to appear more wavy compared to the lower interface. As observed earlier, the breakup occurs at a full-wavelength interval.

So far, the wave number in the present analysis has been taken to be the same for the sinuous and the varicose mode. However, it does not need to be the same because the sinuous and varicose modes satisfy the linearized governing equations and boundary conditions separately and independently. In fact, for a given disturbance of known frequency, the corresponding wavelengths are different for the sinuous and varicose modes. Therefore, in general the wave growth rate and the wave number should be different for

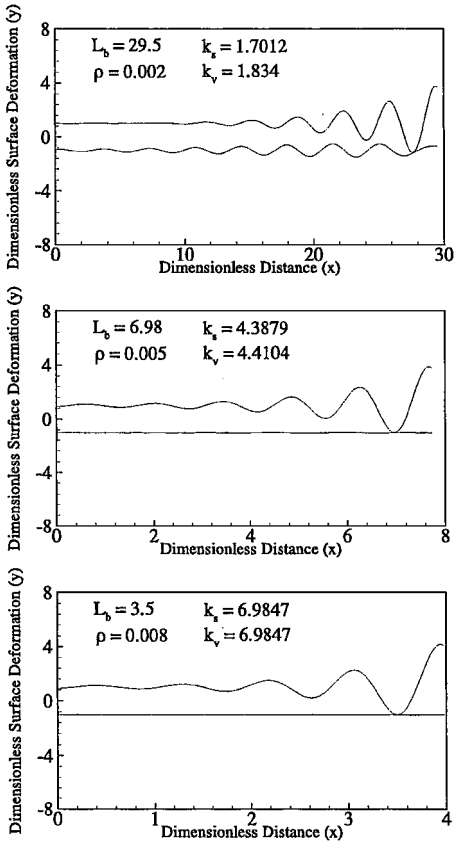

Fig. 10 Spatial surface deformation for $We = 150, Re = 2 \times 10^3, U = 4, \theta = 0, \eta_0 = 0.1, \epsilon_1 = \epsilon_2 = 0.5$, and different values of ρ.

the two unstable modes. As a result, Eq. (16) can be rewritten as follows:

$$\eta_j(x, t) = \eta_0[\epsilon_1 \cosh(\omega_1 t)\cos(\alpha_1 t + k_s x) + (-1)^{j+1}\epsilon_2 \cosh(\omega_2 t)\cos(\alpha_2 t + k_v x + \theta)] \quad (17)$$

where k_s and k_v are the wave numbers for the sinuous and varicose modes, respectively. Figure 3 shows a typical surface evolution at different times. The sheet breakup occurs in between the half- and the full-wavelength interval. This result contrasts with the liquid-sheet breakup at half-wavelength for a sinuous disturbance[14,15] and at a full wavelength for a varicose disturbance.[15]

To obtain a more meaningful representation of the breakup process, the temporal instability formulation, discussed so far, is converted to its spatial counterpart by using Gaster's transformation,[10] which is valid for large Weber numbers.[11] Under such transformation the dimensionless time is equivalent to the dimensionless spatial distance. Figure 4 shows a typical case of interface deformation as the liquid sheet is discharged from the nozzle. The proportion of the sinuous and varicose modes is varied from 25 to 75%. For $\epsilon_1 = 0.75$ and $\epsilon_2 = 0.25$ the liquid sheet coming out of the nozzle has a wavy appearance with the amplitude becoming very large close to the breakup point. However, when the proportion of the varicose mode is increased, the breakup length (or time) is reduced because the time available for the wave growth is shortened, and hence the amplitude at the breakup point is also reduced.

In practice, it is desirable to know the effects of various parameters on the breakup length and breakup characteristics in spray formation. Therefore, in the present study, parameters such as the Reynolds number, Weber number, density ratio, velocity ratio, and phase angle have been varied over a range of values in order to study their influence on the liquid-sheet breakup process. Figure 5 shows the surface evolution at different Reynolds numbers while keeping the other parameters the same as in Fig. 3. The respective dominant wave number for the sinuous and varicose modes, as given in Table 1, is used. It is seen that in Fig. 5a, where $Re = 2 \times 10^2$,

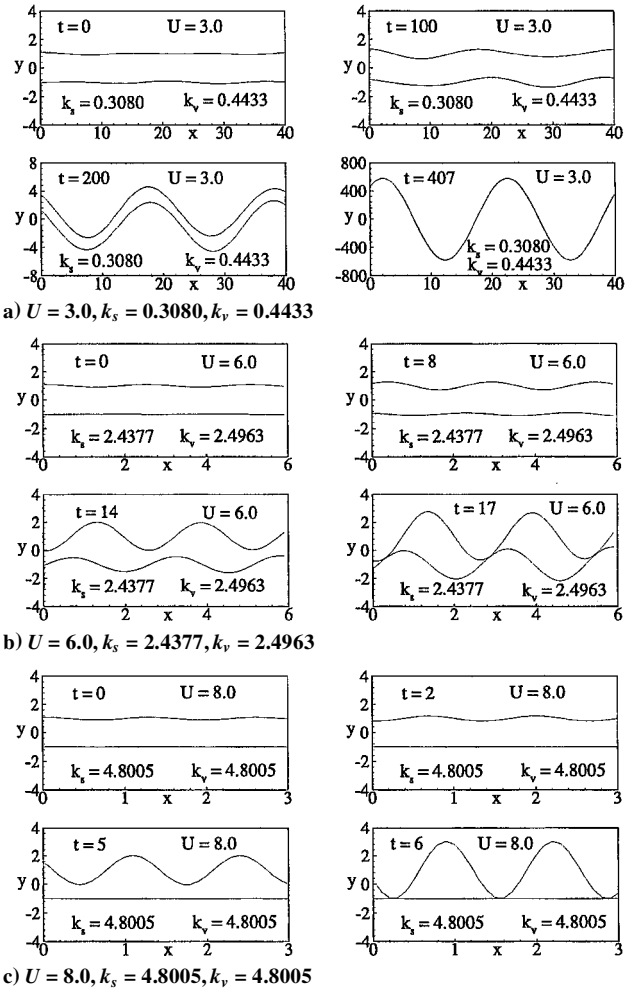

Fig. 11 Evolution of surface deformation for $We = 150, Re = 2 \times 10^3, \rho = 0.001, \theta = 0, \eta_0 = 0.1, \epsilon_1 = \epsilon_2 = 0.5$.

the breakup occurs at $t = 95$, compared to the breakup at $t = 89$ in Fig. 3 for $Re = 2 \times 10^3$. Clearly the viscosity in this case decreases the wave growth rate as shown in Table 1, and therefore it takes more time for the liquid sheet to break up. In Fig. 5b where $Re = 6 \times 10^3$, the breakup occurs earlier at $t = 88$ because in this case the damping effect of viscosity is relatively weak compared to smaller Reynolds numbers. However, the breakup still occurs in between the half- and the full-wavelength interval. Figure 6 shows the spatial evolution of the liquid sheet at different Reynolds numbers. It is evident that with an increase in the Reynolds number the breakup length (or time) is decreased, but the surface profiles remain quite similar for the range of Reynolds numbers investigated.

The surface evolution for different Weber numbers is shown in Fig. 7, and the other parameters are identical to those in Fig. 3. Again the respective dominant wave number for the two unstable modes is used. In Fig. 7a, for We = 100, the two interfaces remain at a constant distance apart for the majority of time and eventually breaking up in between the half- and the full-wavelength at $t = 153$. As given in Table 1, as the Weber number is increased the growth rate of the varicose mode increases at a higher rate compared to the sinuous counterpart. Therefore, the two interfaces grow toward each other more rapidly, which results in shorter breakup time and reduced wave amplitude at the sheet breakup as observed in Figs. 7b and 7c. Similar trends have been observed in experiments as reported by Lefebvre,[18] even though only limited experimental results are available for plane liquid sheets. The spatial development of the interfaces for different Weber numbers is shown in Fig. 8. The breakup length (or time) decreases with an increase in the Weber number and also the surface profiles change at each Weber number.

Figure 9 shows the surface evolution for different density ratios. Figure 9a reveals that for $\rho = 0.002$ the dominant wave number for

the sinuous and varicose modes are very close to each other, resulting in the mutual enhancement of the one surface wave growth and the attenuation of the other surface wave. However, the breakup still occurs in between the half- and the full wavelength interval. At larger density ratios, shown in Figs. 9b and 9c, the breakup point shifts towards the full-wavelength interval. Moreover, the breakup time is also substantially reduced because of the increased growth rate for both unstable modes. At these density ratios not only the dominant wave numbers for the sinuous and varicose modes become almost the same, but also the growth rates for the two unstable modes become comparable, as shown in Table 1. This causes the cancelation of the wave growth at the lower sheet surface and strengthens the growth at the upper surface. Figure 10 shows the corresponding spatial development of the interfacial waves when the density ratio ρ is varied from 0.002 to 0.008. The case for $\rho = 0.001$ is shown in Fig. 4. As discussed earlier, the breakup length (or time) decreases with an increase in the density ratio. Moreover, the surface profiles are significantly different for $\rho = 0.002$ and higher values of ρ. Particularly at $\rho = 0.005$ and 0.008, the upper interface appears much like a free surface wave, and the two surface profiles are extremely unsymmetrical because of the superposition and cancellation of the sinuous and varicose waves discussed earlier.

Figure 11 shows the surface evolution at different velocity ratios. It takes a long time for the liquid sheet to break up at a velocity ratio of 3.0 as shown in Fig. 11a as compared to Fig. 11b for $U = 6.0$. A similar observation is also reported by Lefebvre[18] for the breakup of flat sheets in a coflowing airstream. This is because the growth rate of the varicose mode is much smaller (almost two orders of magnitude smaller) than the sinuous mode at the velocity ratio of three, as given in Table 1. As a result, the sinuous mode leads to substantial wave growth before the sheet breakup, which is caused by the varicose mode. The wave amplitude at the breakup is substantially reduced with an increase in the surrounding gas velocity because of a significant increase in the growth rate of the varicose mode given in Table 1. However, for $U = 8.0$ the dominant wave numbers and the wave growth rates for the two unstable modes become almost identical, as given in Table 1. Consequently, Fig. 11c shows that the wave growth strengthens at the upper interface and cancels out at the lower interface because of the superposition of the sinuous and varicose mode. Such a phenomenon has also been observed earlier. Figure 12 shows the spatial development of the interface at different velocity ratios. The breakup length (or time) is substantially reduced at a high gas velocity. The case for $U = 8.0$,

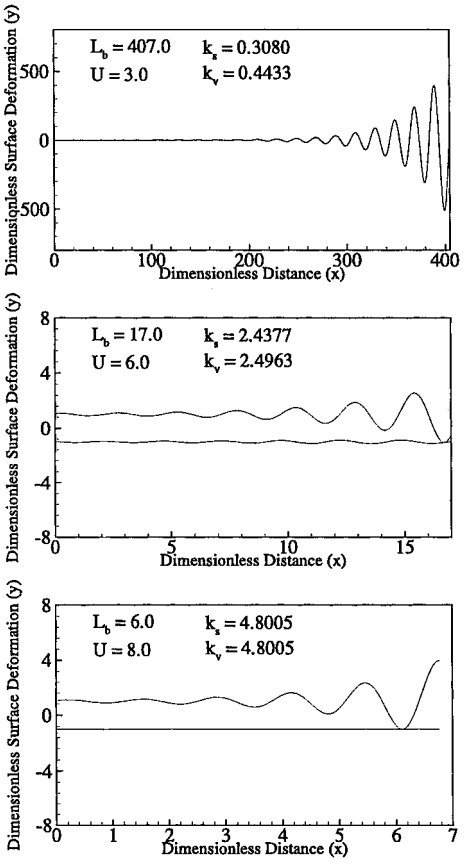

Fig. 12 Spatial surface deformation for $We = 150$, $Re = 2 \times 10^3$, $\rho = 0.001$, $\theta = 0$, $\eta_0 = 0.1$, $\epsilon_1 = \epsilon_2 = 0.5$, and different values of U.

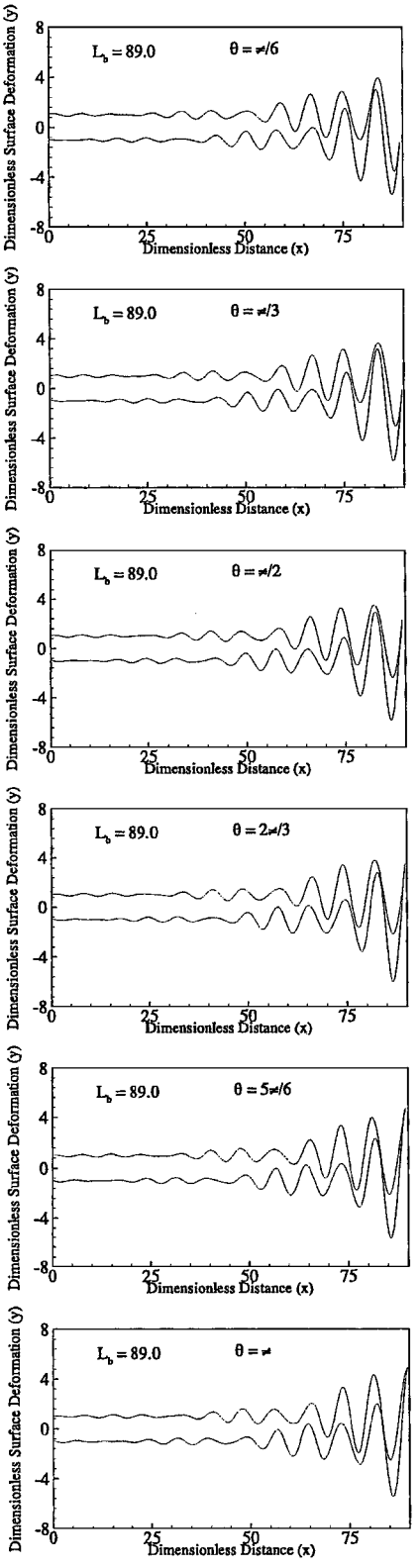

Fig. 13 Spatial surface deformation for $We = 150$, $Re = 2 \times 10^3$, $\rho = 0.001$, $\eta_0 = 0.1$, $k_s = 0.7561$, $k_v = 0.9651$, $\epsilon_1 = \epsilon_2 = 0.5$, and different phase angle θ.

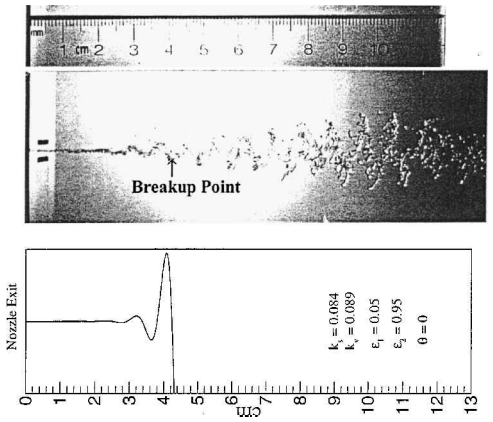

Fig. 14 Comparison of the surface deformation obtained by the present linear analysis with the experimental photograph at 1.12-kHz excitation.[19] $We = 169.38$, $Re = 4729.37$, $\rho = 1.2 \times 10^{-3}$, $U = 4.76$, $k_s = 0.084$, $k_v = 0.089$, $\epsilon_1 = 0.05$, $\epsilon_2 = 0.95$, and $\eta_0 = 0.6$.

the upper interface evolution, appears much like a free surface wave, similar to the case observed earlier for a high density ratio.

Figure 13 shows the effect of the phase angle on the surface evolution. The phase angle θ is varied from $\pi/6$ to π. The surface evolution for the case $\theta = 0$ is shown in Fig. 4. In all of these cases, the sinuous mode tries to grow, which is seen by a substantial increase in an amplitude further downstream from the nozzle exit, whereas the varicose mode tends to bring the two interfaces close together, which eventually leads to the breakup of the liquid sheet. The breakup length (or time) remains more or less the same for different phase angles, but the surface profiles change progressively with the phase angle between the two unstable modes.

The present analysis has been compared with the experimental results by Jazayeri and Li,[19] and a typical case is shown in Fig. 14. In the experiment a two-dimensional nozzle was used to produce a liquid (water) sheet, 254 μm thick, moving with a velocity of 9.78 m/s in a coflowing gas (air) stream of velocity 46.55 m/s, and an external acoustic excitation of 1.12-kHz frequency was imposed on the sheet in order to obtain a well-defined wave form. The flow parameters are $We = 169.38$, $Re = 4729.37$, $U = 4.76$, and $\rho = 1.2 \times 10^{-3}$. The wave numbers of $k_s = 0.084$ and $k_v = 0.089$ are the respective wave numbers of the sinuous and varicose modes corresponding to the disturbance frequency of 1.12 kHz. The initial amplitude of disturbance is taken as 0.6. Even though such a large value of the initial amplitude does not represent a small parameter needed in the linear stability analysis, it is required in order to match experimental results with the linear theory, as also found by Asare et al.[20] It is seen in Fig. 14 that the predicted liquid sheet remains more or less flat for a significant distance downstream of the nozzle exit (over 2.5 cm), then the waves grow very quickly with the sheet breakup at a distance of 4.2 cm from the nozzle exit, as compared to around 4 cm shown in photograph. Even though the predicted surface deformation close to the nozzle exit matches with that observed in the photograph, a large deviation occurs near the breakup point. Such deviation for the linear theory can be attributed to the fact that nonlinear effects become dominant near the breakup region. The nonlinearity will slow down the growth of the sinuous mode and decrease the wave amplitude at the breakup region, as observed in the photograph. Therefore, it is imperative to extend the present analysis to include the nonlinear effects in order to describe more accurately the breakup characteristics of the plane liquid sheets.

Conclusion

The breakup process of a plane viscous liquid sheet in a gas stream has been investigated by linear stability analysis subject to the combined influence of sinuous and varicose modes. At a wave number corresponding to the dominant wave number of either the sinuous or the varicose modes, the breakup occurs at a full-wavelength interval. The sinuous mode is responsible for the development of large amplitude deformation, whereas the varicose mode is responsible for the breakup of the liquid sheet. The breakup time (or length) decreases with an increase in the proportion of the varicose mode in the initial disturbance. When the respective dominant wave numbers for the sinuous and varicose modes are applied simultaneously, the breakup occurs between the half- and the full-wavelength interval. However at higher density and velocity ratios, when the dominant wave numbers and the growth rates of the two modes are comparable, the breakup shifts to the full-wavelength interval. The breakup length decreases with an increase in the Reynolds number, Weber number, density ratio, and velocity ratio, but it remains more or less the same at different phase angles between the two modes. These results agree with the known experimental observations. Except for different Reynolds numbers, surface profiles are distinctly different at each Weber number, density ratio, velocity ratio, and phase angle. Comparison of the present linear theory with the experimental results shows that the predicted surface deformation agrees favorably with the experiment, but significant deviation occurs near the sheet breakup region, necessitating a nonlinear analysis for a better description of the sheet breakup process.

Acknowledgment

The financial support of the Natural Sciences and Engineering Research Council of Canada is greatly appreciated.

References

[1]Shen, J., and Li, X., "Instability of an Annular Viscous Liquid Jet," *Acta Mechanica*, Vol. 114, Nos. 1–4, 1996, pp. 167–183.

[2]Shen, J., and Li, X., "Breakup of Annular Viscous Liquid Jets in Two Gas Streams," *Journal of Propulsion and Power*, Vol. 12, No. 4, 1996, pp. 752–759.

[3]Mitra, S. K., and Li, X., "A Predictive Model for Droplet Size Distribution in Sprays," *Atomization and Sprays*, Vol. 9, No. 1, 1999, pp. 29–50.

[4]Squire, H. B., "Investigation of the Instability of a Moving Film," *British Journal of Applied Physics*, Vol. 4, June 1953, pp. 167–169.

[5]Hagerty, W. W., and Shea, J. F., "Investigation of the Instability of a Moving Film," *Journal of Applied Mechanics*, Vol. 22, No. 4, 1955, pp. 509–514.

[6]Li, X., and Tankin, R. S., "On the Temporal Instability of a Two-Dimensional Viscous Liquid Sheet," *Journal of Fluid Mechanics*, Vol. 226, May 1991, pp. 425–443.

[7]Lin, S. P., Lian, Z. W., and Creighton, B. J., "Absolute and Convective CInstability of a Liquid Sheet," *Journal of Fluid Mechanics*, Vol. 220, Nov. 1990, pp. 673–689.

[8]Li, X., "Spatial Instability of Plane Liquid Sheet," *Chemical Engineering Science*, Vol. 48, No. 16, 1993, pp. 2973–2981.

[9]Teng, C. H., Lin, S. P., and Chen, J. N., "Absolute and Convective Instability of a Viscous Liquid curtain in a Viscous Gas," *Journal of Fluid Mechanics*, Vol. 332, Feb. 1997, pp. 105–120.

[10]Gaster, M., "A Note on the Relation Between Temporally-Increasing and Spatially-Increasing Disturbances in Hydrodynamic Stability," *Journal of Fluid Mechanics*, Vol. 14, Pt. 2, 1964, pp. 222–224.

[11]Li, X., *Mixed-Flow Hydrodynamics*, Advances in Engineering Fluid Mechanics, Gulf Publishing Co., Houston, TX, 1996, pp. 145–166.

[12]Clark, C. J., and Dombrowski, N., "Aerodynamic Instability and Disintegration of Inviscid Liquid Sheets," *Proceedings of Royal Society of London, A*, Vol. 329, No. 1579, 1972, pp. 467–478.

[13]Rangel, R. H., and Sirignano, W. A., "Nonlinear Growth of Kelvin-Helmholtz Instability: Effect of Surface tension and Density Ratio," *Physics of Fluids*, Vol. 31, No. 7, 1988, pp. 1845–1855.

[14]Jazayeri, S. A., and Li, X., "Nonlinear Instability of Plane Liquid Sheets," *Journal of Fluid Mechanics*, Vol. 406, March 2000, pp. 281–308.

[15]Mitra, S. K., Li, X., and Renksizbulut, M., "Nonlinear Breakup of Plane Liquid Sheets in a Co-Flowing Gas Stream," (to be published).

[16]Li, X., "On the Instability of Plane Liquid Sheets in Two Gas Streams of Unequal Velocities," *Acta Mechanica*, Vol. 106, Nos. 3, 4, 1994, pp. 137–156.

[17]Muller, D. E., "A Method for Solving Algebraic Equations Using an Automatic Computer," *Mathematical Tables and Other Aid to Computation*, Vol. 10, No. 5, 1956, pp. 208–215.

[18]Lefebvre, A. H., *Atomization and Sprays*, Hemisphere, New York, 1989.

[19]Jazayeri, S. A., and Li, X., "Structures of Liquid-Sheet Sprays," *Particle and Particle System Characterization*, Vol. 17, No. 2, 2000, pp. 56–65.

[20]Asare, H. R., Takahashi, R. K., and Hoffman, M. A., "Liquid Sheet Jet Experiments: Comparison with Linear Theory," *Journal of Fluids Engineering*, Vol. 103, No. 4, 1981, pp. 595–604.